INTERNATIONAL COMPARISON OF MEASUREMENTS OF NEUTRON SOURCE EMISSION RATE (2016-2021) – CCRI(III)-K9.Cf.2016

Z. Vykydal
Czech Metrological Institute (CMI), Praha, Czech Republic

H. Park and J. Kim
Korea Research Institute of Standards and Science (KRISS), Daejeon, Republic of Korea

W.W. Pereira and E.S. da Fonseca
National Laboratory of Metrology of Ionizing Radiation (IRD/LNMRI), Rio de Janeiro, Brazil

C. Thiam
Université Paris-Saclay, CEA, List, Laboratoire National Henri Becquerel (LNE-LNHB), F-91120, Palaiseau, France

Zhang Hui

National institute of Metrology (NIM), Beijing, China

M.S. Dewey and H.P. Mumm
National Institute of Standards and Technology (NIST), Gaithersburg, USA

H. Harano, T. Matsumoto, A. Masuda, and S. Manabe

National Metrology Institute of Japan (NMIJ), Tsukuba, Japan

N.J. Roberts* and N.A. Horwood
National Physical Laboratory (NPL), Teddington, UK

J.P. Archambault

National Research Council (NRC), Ottawa, Canada

N.N. Moiseev and A.V. Didyk
D.I. Mendeleyev Institute for Metrology (VNIIM), St. Petersburg, Russia

* corresponding author: neil.roberts@npl.co.uk

ABSTRACT

Section III (neutron measurements) of the Comité Consultatif des Rayonnements Ionisants, CCRI, conducted a comparison of primary measurements of the neutron emission rate of a ^{252}Cf radionuclide source. A single ^{252}Cf source was circulated to all participants between 2016 and 2020. Ten laboratories participated –CMI (Czech Republic), KRISS (Republic of Korea), IRD/LNMRI (Brazil), LNE-LNHB (France), NIM (China), NIST (USA), NMIJ (Japan), NPL (UK), NRC (Canada) and VNIIM (Russia) – with NPL making their measurements at the start and repeating them at the end of the exercise to verify the ^{250}Cf content of the source. Each laboratory reported the emission rate into 4π sr together with a detailed uncertainty budget. All participants used the manganese bath technique except NMIJ who used a relative method based on measurements with a ^{3}He detector in a graphite pile. VNIIM also made measurements using an associated particle technique. CMI, KRISS, LNE-LNHB, NIM, NPL and VNIIM also measured the anisotropy of the source although this did not formally form part of the comparison.

TABLE OF CONTENTS

1 INTRODUCTION

Intercomparisons of neutron source emission rate are staged infrequently and typically take many years to perform. The only previous comparisons involving large numbers of participants were those carried out between 1959 and 1965 involving a Ra-Be(α,n) source[1], between 1979 and 1984 involving three different ^{252}Cf sources[2], and between 1999 and 2005 involving a ^{241}Am-Be(α,n) source. It is the aim of Section III of the CCRI to compare the realisation of standards of all relevant neutron quantities over a ten-year cycle, so it was decided to arrange a new intercomparison of neutron source emission rate. Ten laboratories participated and they were:

Czech Metrological Institute (CMI), Praha, Czech Republic

Korea Research Institute of Standards and Science (KRISS), Daejeon, Republic of Korea

National Laboratory of Metrology of Ionizing Radiation (LNMRI), Rio de Janeiro, Brazil

Laboratoire National Henri Becquerel (LNE-LNHB), Gif-sur-Yvette, France

National Institute of Metrology (NIM), Beijing, China

National Institute of Standards and Technology (NIST), Gaithersburg, USA

National Metrology Institute of Japan (NMIJ), Tsukuba, Japan

National Physical Laboratory (NPL), Teddington, UK

National Research Council (NRC), Ottawa, Canada

D.I. Mendeleyev Institute for Metrology (VNIIM), St. Petersburg, Russia

2 THE ^{252}Cf RADIONUCLIDE SOURCE

The neutron source used was a sealed ^{252}Cf(sp.f.) source (model CVN.CY2, serial number 51227B) owned by NPL, which had a nominal activity of 100 MBq in 2015. It is in an X1 capsule (outer length 10 mm, outer diameter 7.8 mm) and was manufactured by QSA Global, Inc.

The source was chosen because it is representative of the type and size of neutron sources commonly used at the present time in calibration laboratories, and is different from the source type used in the previous comparison exercise. In the K9.AmBe comparison there was some divergence of results due to the different choices of cross-section library used to calculate the O(n,α) capture fraction made by participants. As the O(n,α) capture fraction is smaller for ^{252}Cf sources than for ^{241}Am-Be sources, the choice of cross-section library should be less significant and lead to a higher level of agreement between participants. After NPL had made the first measurement the source was sent to each participant in turn. NPL coordinated the scheduling of participants with each laboratory responsible for sending the source on to the next participant.

In 2022, at the end of the exercise, the source returned to NPL for a repeat measurement. This was in order for the decay of the source over the period of the comparison exercise to be determined by allowing for the presence of ^{250}Cf which also produces neutrons via spontaneous fission.

3 ASSESSMENT OF ^{250}Cf CONTENT

The information sheet supplied by Oak Ridge when the Pd-Cf_2O_3 composite wire used in source 51227B was supplied to QSA Global[3] contains the isotopic analysis data given in Table 1. The ^{248}Cm decay product was last separated on 30 October 2009.

Table 1 Isotopic mass analysis of Cf batch code CXCF-780 used to make source 51227B, dated 11 June 2009

Nuclide	Isotopic composition (wt%)
^{249}Cf	6.985
^{250}Cf	9.807
^{251}Cf	3.037
^{252}Cf	80.167
^{253}Cf	0.003
^{254}Cf	0.003

The neutron emission rate of a californium source as a function of time is given by the following equation[4]:

$$Q = R\ exp(-\lambda_{252}t) + S\,exp(-\lambda_{250}t) + T[1 - exp(-\lambda_{252}t)] \qquad (1)$$

where Q is the neutron emission rate of the source at time t,
R is the neutron emission rate from the ^{252}Cf component at time $t = 0$,
t is the time in days from the reference date,
λ_{252} is the decay constant for ^{252}Cf and this is related to the half-life, t_{252}, by $\lambda_{252} = \ln(2) / t_{252}$ ($t_{252} = 966.1$ days[5]),
S is the neutron emission rate from the ^{250}Cf component at time $t = 0$,
λ_{250} is the decay constant for ^{250}Cf and this is related to the half-life, t_{250}, by $\lambda_{250} = \ln(2) / t_{250}$ ($t_{250} = 4777$ days[5]),
T is the neutron emission rate from ^{248}Cm when all the ^{252}Cf has decayed.

The content of ^{248}Cm in 51227B over the period of the comparison measurements will be negligible given the relatively recent separation date, so equation 1 can be simplified to:

$$Q = R\ exp(-\lambda_{252}t) + S\,exp(-\lambda_{250}t) \qquad (2)$$

The ratio of the ^{250}Cf to ^{252}Cf present in the source as a function of time can be obtained from the following equation[4]:

$$\frac{N(^{250}Cf)}{N(^{252}Cf)} = \frac{S\exp(-\lambda_{250}t)}{R\exp(-\lambda_{252}t)}\frac{t_{250}}{t_{252}}\frac{B_{252}}{B_{250}}\frac{\bar{\nu}_{252}}{\bar{\nu}_{250}} \qquad (3)$$

where: N(x) is the number of nuclei of isotope x at time t,
B_{252} is the branching ratio for spontaneous fission in ^{252}Cf (= 0.03102[6]),
B_{250} is the branching ratio for spontaneous fission in ^{250}Cf (= 0.00077[6]).
$\bar{\nu}_{250}$ is the average number of neutrons emitted per spontaneous fission event in ^{250}Cf (= 3.51[7])
$\bar{\nu}_{252}$ is the average number of neutrons emitted per spontaneous fission event in ^{252}Cf (= 3.7655[8])

The ratio of the neutron emission rates from ^{252}Cf to ^{250}Cf at time $t = 0$ can therefore be obtained using the percentages of each nuclide given in the isotopic analysis, taking the date of the

analysis as $t = 0$:

$$\frac{R}{S} = \frac{N(^{252}Cf)}{N(^{250}Cf)} \frac{t_{250}}{t_{252}} \frac{B_{252}}{B_{250}} \frac{\bar{\nu}_{252}}{\bar{\nu}_{250}} \qquad (4)$$

Using Table 1 we obtain a value for the ratio of 1.732×10^3 which can be used to determine both R and S in equation 2 by fitting to the two NPL measurements. Both NPL measurements can then be decay corrected back to the reference date of the comparison exercise (1/1/2016) using the isotopic analysis data to allow for the ^{250}Cf component. The decay corrected values obtained using the fit and using only the ^{252}Cf half-life, normalised to the respective mean value, are plotted in Figure 1. The agreement of the two measurements is much better when the fit based on the isotopic analysis is used rather than only using the ^{252}Cf half-life (<0.004% compared to 0.89%) showing that the NPL measurements are consistent with the isotopic analysis. The random uncertainties in the measurements are 0.35% at $k = 1$, so the two NPL measurements could be said to be in agreement even if the ^{252}Cf half-life is used to decay correct them. This demonstrates that the ^{250}Cf correction is very small and could not be properly determined using only the NPL emission rate data.

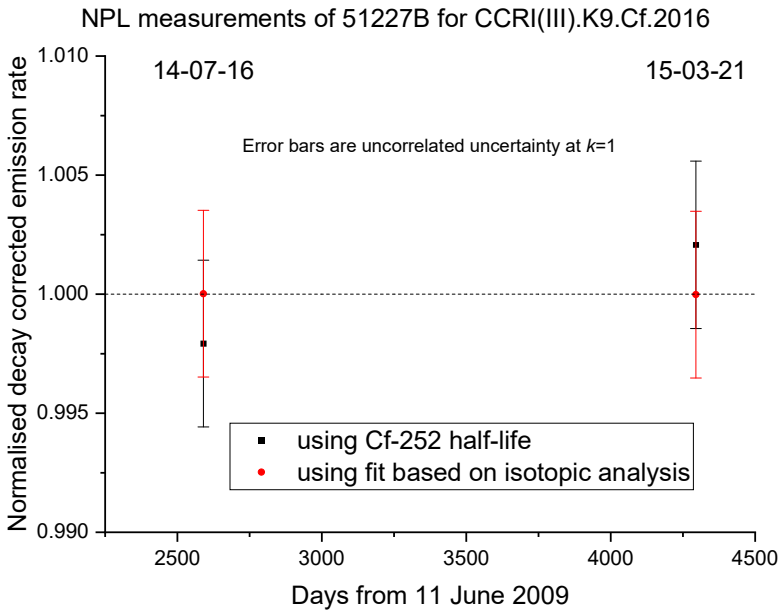

Figure 1: Normalised values for the source emission rate decay corrected to the reference date of the comparison, using the ^{252}Cf half-life and the fit based on the isotopic analysis which allows for the ^{250}Cf component

A correction factor, C, can be defined to correct the measurements made in the comparison for the presence of ^{250}Cf to the reference date of 1/1/2016 (2395 days from the date of the isotopic analysis) using the fit to the isotopic analysis data. As the protocol instructed each participant to perform a decay correction using only the ^{252}Cf half-life, the correction factor includes a term to remove this correction.

$$C = \frac{R\ exp(-\lambda_{252} \times 2395) + S\ exp(-\lambda_{250} \times 2395)}{R\ exp(-\lambda_{252} t) + S\ exp(-\lambda_{250} t)} \times \frac{1}{exp(\lambda_{252} t')} \qquad (5)$$

where: t' is the number of days from the emission rate measurement to the reference date of the comparison.

The percentage correction to the reported emission rate (= C-1) is plotted as a function of time for the duration of the comparison exercise in Figure 2. Each participant is indicated on the curve at the time of their measurement.

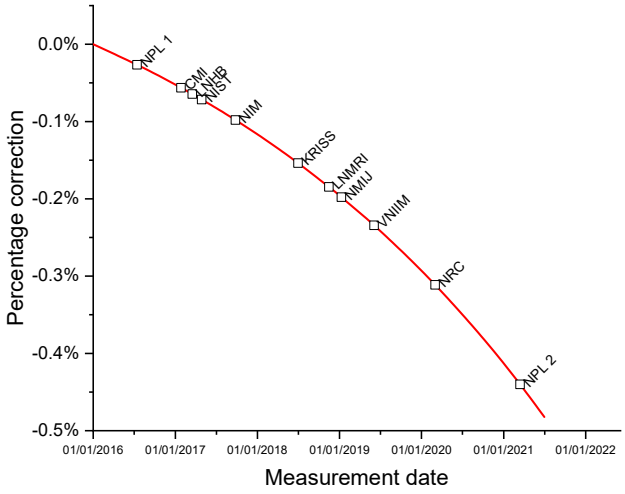

Figure 2: Percentage ^{250}Cf correction over the measurement phase of the K9.Cf.2016 comparison exercise

4 NEUTRON EMISSION RATE MEASUREMENT TECHNIQUES OF THE LABORATORIES

Nine of the ten participants used the manganese bath technique with the VNIIM additionally using a method based on an associated particle technique. The only institute not to use the manganese bath technique was the NMIJ who used a relative method traceable to NPL. Further details of the techniques used by each institute, taken from their comparison reports, are given in Appendix C.

The features of all nine manganese bath facilities are listed in Table 2.

Table 2: Summary of manganese bath parameters

Laboratory	Bath size	N_H/N_{Mn} at time of measurement	Correction factor method	ENDF oxygen library	Impurities considered?	Activity counting system
CMI	100 cm diameter	63.33	MCNP 6.1.1	B-VII.1	Yes	Static detector in bath
KRISS	125 cm diameter	179.11	MCNPX 2.7.0	B-VII	No	Circulation of solution
LNMRI	100 cm diameter	35.26	MCNPX 2.7.0	B-VI	No	Static detector in bath
LNE-LNHB	100 cm diameter	52.2	MCNP 6	B-VII	No	Circulation of solution
NIM	110 cm diameter	59.704	MCNP 4C	B-VII	No	Circulation of solution
NIST	129 cm diameter	57.55	MCNP 6.2	B-VI	No*	Circulation of solution
NPL	98 cm diameter	34.37	MCNP 5 +thermal calculation	B-VI	Yes	Circulation of solution
NRC	100 cm diameter	46.6	MCNP 6 +thermal calculation	B-VII.1	No	Static detector at top of bath
VNIIM	85 cm diameter cylinder	48.89	MCNP 4C	B-VI	Yes	Static detector in bath

* Due to the ratio method used by the NIST the effect of any impurities is considered to cancel.

5 RESULTS

The emission rates submitted by each participant with uncertainties at $k = 2$ with the associated reference dates, measurement dates and ^{250}Cf correction factors are given in Table 3. As defined in the measurement protocol, all have been corrected to the reference date of 1st January 2016.

Table 3: Emission rates on the stated reference dates as reported by the participants with uncertainties at $k = 2$, and calculated ^{250}Cf correction factors corresponding to the stated measurement dates

Laboratory	Reported emission rate ($\times 10^7$ s^{-1})	Uncertainty [$k = 2$] ($\times 10^7$ s^{-1})	Reference date used (dd/mm/yyyy)	Measurement date used for ^{250}Cf correction	^{250}Cf correction factor
CMI	1.256	0.0098	01/01/2016	26/01/2017	0.99944
KRISS	1.263	0.0215	01/01/2016	01/07/2018	0.99846
LNE-LNHB	0.9030	0.0240	17/03/2017	17/03/2017	0.99936
LNMRI	1.271	0.0190	01/01/2016	15/11/2018	0.99815
NIM	1.257	0.0189	01/01/2016	25/09/2017	0.99902
NIST	1.249	0.0220	01/01/2016	28/04/2017	0.99928
NMIJ	1.252	0.0396	01/01/2016	10/01/2019	0.99802
NPL*	1.247	0.0130	01/01/2016	14/07/2016	0.99973
NRC	1.290	0.0400	01/01/2016	02/03/2020	0.99689
VNIIM Mn bath	0.5153	0.0063	04/06/2019	04/06/2019	0.99766
VNIIM AP	0.5126	0.0063	04/06/2019	04/06/2019	0.99766

The emission rates corrected to the reference date of 1st January 2016 and multiplied by the ^{250}Cf correction factor for the date of the measurement are given in Table 4.

Table 4: Emission rates corrected to 1st January 2016 with uncertainties at $k = 2$

Laboratory	Emission rate ($\times 10^7$ s^{-1})	Uncertainty [$k = 2$] ($\times 10^7$ s^{-1})
CMI	1.2549	0.0098
KRISS	1.2611	0.0215
LNE-LNHB	1.2383	0.0329
LNMRI	1.2687	0.0190
NIM	1.2558	0.0189
NIST	1.2481	0.0220
NMIJ	1.2499	0.0396
NPL*	1.2467	0.0130
NRC	1.2860	0.0400
VNIIM†	1.2572	0.0154

* The NPL value is from the 2016 measurement only.

† The VNIIM value is a mean of the manganese bath and associated particle measurements.

6 ANALYSIS OF RESULTS

The evaluation of the key comparison data has been carried out following Procedure A as outlined by Cox[9]. The weighted mean was determined using the inverses of the squares of the associated standard uncertainties as the weights but excluding the result of NMIJ as it is traceable to that of NPL. The standard deviation was determined from the inverse of the sum of the weights. This gave a weighted mean of 1.2550×10^7 s^{-1} and a weighted mean uncertainty of 0.0028×10^7 s^{-1} (0.22 %). The standard deviation is 0.0138×10^7 s^{-1} (1.10 %) and the SEOM is 0.0046×10^7 s^{-1} (0.37 %). The results are plotted in Figure 3 with expanded uncertainties together with the weighted mean.

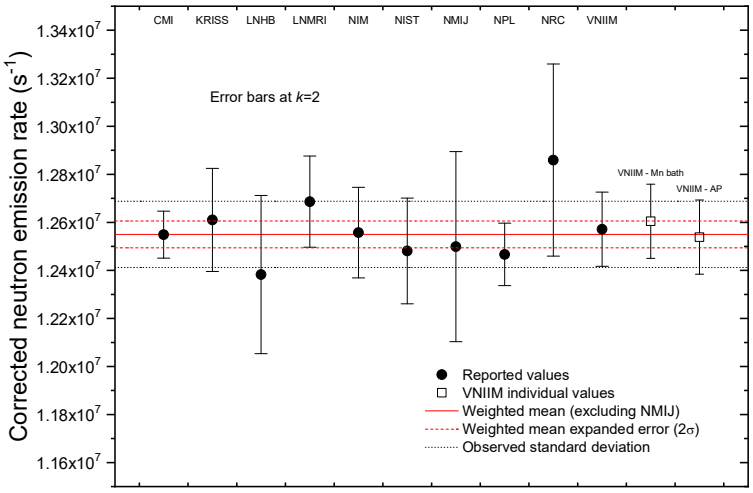

Figure 3: Graph of emission rates with uncertainties at $k = 2$

A chi-squared test was applied as an overall consistency check of the results. The χ^2 contribution for each participant is defined as $d^2/u(\text{measured value})^2$, where d is the difference between the measured value and the weighted mean. The χ^2 contributions for each participant are given in Table 5. The observed chi-squared value was formed from the sum of the χ^2 contributions, excluding that of NMIJ, and yielded a value of 7.936. The chi-squared value for a probability of 0.05 with 8 degrees of freedom must be less than 15.5 to pass the consistency check, so the data presented here can be regarded as consistent.

Table 5: χ^2 contributions for all participants

Laboratory	χ^2 contribution
CMI	0.001
KRISS	0.313
LNE-LNHB	1.036
LNMRI	2.051
NIM	0.006
NIST	0.398
NMIJ	0.067
NPL	1.662
NRC	2.392
VNIIM	0.076

7 SUMMARY AND CONCLUSION

Ten institutes have submitted values for the emission rate of the ^{252}Cf source. Nine used the manganese bath technique with the VNIIM additionally using a method based on an associated particle technique, and the NMIJ using a relative method traceable to NPL. There is excellent agreement between all the values resulting in an observed χ^2 value of 7.936, a weighted mean of 1.2550×10^7 s^{-1} with a weighted mean uncertainty of 0.0028×10^7 s^{-1} (0.22 %) and a SEOM of 0.0046×10^7 s^{-1} (0.37 %).

The overall spread of the results is similar to the previous key comparison exercise involving an Am-Be source. The use of a ^{252}Cf source for this comparison, which involves a much smaller correction for the O(n,α) capture component in the manganese sulphate solution and so is less influenced by the nuclear data libraries chosen by each participant, has not impacted the overall level of agreement.

8 ACKNOWLEDGEMENTS

The authors would like to thank Dr Steven Judge and Dr Vincent Gressier for their help with setting up, running and evaluating the exercise.

The evaluation of the intercomparison was supported by the National Measurement System of the UK government's Department for Science, Innovation and Technology.

9 APPENDICES

9.1 Appendix A: Reference value and degrees of equivalence

The proposed KCRV has been calculated by taking a weighted mean of the results submitted by the participants, excluding NMIJ who obtain traceability from NPL. The KCRV and its uncertainty are given in Table 6.

Table 6: Proposed values for the KCRV with standard uncertainty

KCRV	$1.2550 \times 10^{7}\ \mathrm{s}^{-1}$
u(KCRV)	$0.0028 \times 10^{7}\ \mathrm{s}^{-1}$

With x_{ref} corresponding to the KCRV, the unilateral degree of equivalence (DoE) of participant i is formed from the pair of values $(d_i, U(d_i))$ using the following equations:

$$d_i = x_i - x_{ref}$$

$$U(d_i) = 2u(d_i)$$

where $U(d_i)$ is the expanded uncertainty using a coverage factor of 2 to give 95% coverage under the assumption of normality, and $u(d_i)$ is given by

$$u^2(d_i) = u^2(x_i) - u^2(x_{ref}),$$

except for those points which were excluded from the determination of the KCRV for which $u(d_i)$ is given by

$$u^2(d_i) = u^2(x_i) + u^2(x_{ref}).$$

The DoE values, χ^2 contributions, and E-values using the weighted mean from the LCS are given in Table 7. The E-value is defined as $d_i/u(d_i)$.

Table 7: Unilateral DoE values, χ^2 contributions and E-values

Laboratory	Unilateral DoE		χ^2 contribution	E-value
	d_i ($\times 10^7$ s^{-1})	$U(d_i)$ ($\times 10^7$ s^{-1})		
CMI	-0.0002	0.0080	0.001	-0.039
KRISS	0.0060	0.0207	0.313	0.580
LNE-LNHB	-0.0168	0.0325	1.036	-1.033
LNMRI	0.0136	0.0182	2.051	1.499
NIM	0.0007	0.0180	0.006	0.080
NIST	-0.0069	0.0213	0.398	-0.653
NMIJ	-0.0051	0.0400	0.067	-0.257
NPL	-0.0084	0.0117	1.662	-1.429
NRC	0.0309	0.0396	2.392	1.562
VNIIM	0.0021	0.0144	0.076	0.297

The degree of equivalence, $(d_{i,j},U(d_{i,j}))$ between participant i and participant j, is formed using the following equations:

$$d_{i,j} = x_i - x_j$$

$$U(d_{i,j}) = 2u(d_{i,j})$$

where $u(d_{i,j})$ is given by

$$u^2\left(d_{i,j}\right) = u^2\left(x_i\right) + u^2\left(x_j\right).$$

The degrees of equivalence between pairs of participants are given in Table 8.

Table 8: Degrees of equivalence between pairs of participants

Laboratory	$(d_{i,j}, U(d_{i,j}))$ ($\times 10^6$ s^{-1})									
j \ i	CMI	KRISS	LNE-LNHB	LNMRI	NIM	NIST	NMIJ	NPL	NRC	VNIIM
CMI	-	0.062,0.236	-0.166,0.344	0.138,0.214	0.009,0.212	-0.068,0.241	-0.050,0.408	-0.082,0.163	0.311,0.412	0.023,0.183
KRISS	-0.062,0.236	-	-0.228,0.393	0.076,0.287	-0.053,0.286	-0.130,0.307	-0.111,0.450	-0.144,0.251	0.249,0.454	-0.039,0.265
LNE-LNHB	0.166,0.344	0.228,0.393	-	0.304,0.380	0.175,0.379	0.098,0.396	0.116,0.515	0.084,0.354	0.477,0.518	0.189,0.364
LNMRI	-0.138,0.214	-0.076,0.287	-0.304,0.380	-	-0.129,0.268	-0.205,0.291	-0.187,0.439	-0.220,0.230	0.173,0.443	-0.115,0.245
NIM	-0.009,0.212	0.053,0.286	-0.175,0.379	0.129,0.268	-	-0.077,0.290	-0.058,0.438	-0.091,0.229	0.302,0.442	0.014,0.244
NIST	0.068,0.241	0.130,0.307	-0.098,0.396	0.205,0.291	0.077,0.290	-	0.018,0.453	-0.014,0.256	0.379,0.457	0.091,0.269
NMIJ	0.050,0.408	0.111,0.450	-0.116,0.515	0.187,0.439	0.058,0.438	-0.018,0.453	-	-0.033,0.417	0.361,0.563	0.073,0.425
NPL	0.082,0.163	0.144,0.251	-0.084,0.354	0.220,0.230	0.091,0.229	0.014,0.256	0.033,0.417	-	0.393,0.421	0.105,0.202
NRC	-0.311,0.412	-0.249,0.454	-0.477,0.518	-0.173,0.443	-0.302,0.442	-0.379,0.457	-0.361,0.563	-0.393,0.421	-	-0.288,0.429
VNIIM	-0.023,0.183	0.039,0.265	-0.189,0.364	0.115,0.245	-0.014,0.218	-0.091,0.269	-0.073,0.425	-0.105,0.202	0.288,0.429	-

9.2 Appendix B: Uncertainty budgets of the participants

9.2.1 Uncertainties reported by CMI

Table 9: Component uncertainties for CMI Mn bath measurement

Source of uncertainty	Value (%)	Probability distribution	Divisor	Relative sensitivity	Uncertainty component (± %)	Degrees of freedom
Fitted count rate N_0	0.037	Normal	1	1	0.037	700
Probability of neutron absorption by Mn ε_1	0.34	Normal	1	1	0.335	50
Counter efficiency ε_2	0.16	Normal	1	1	0.160	50
Time of irradiation T_1	0.022	Rectangular	√3	0.01	Neglected	Inf
Time of stirring T_2	0.47	Rectangular	√3	0.16	0.043	Inf
Time of reference T_R	3.0E-5	Rectangular	√3	0.28	Neglected	Inf
Half-life of ^{56}Mn	0.19	Normal	1	0.17	0.031	5000
Half-life of ^{252}Cf	0.30	normal	1	0.28	0.085	5000
Combined uncertainty					0.39	84

9.2.2 Uncertainties reported by KRISS

Table 10: Component uncertainties for KRISS Mn bath measurement

	Source of uncertainty	Value (±)	Probability distribution	Divisor	c_i	u_i (± %)	v_i or v_{eff}
Measurement in year 2018	Fit parameter for N_{sat}	0.12%	normal	1	1	0.12%	∞
	Fit parameter for N^r_{sat}	0.30%	normal	1	1	0.30%	∞
Emission rate of ref neutron source (measurement in year 2009)	Fit parameter for N_{sat}	0.40%	normal	1	1	0.40%	∞
	Half-life of ^{241}Am-Be	0.14%	normal	1	0.008	0.00%	∞
	Cross section for ε_{Mn}	0.50%	normal	1	1	0.50%	∞
	H/Mn ratio for ε_{Mn}	0.15%	normal	1	1	0.15%	∞
	Activity of standard ^{56}Mn	0.38%	normal	1	1	0.38%	∞
	Mass of ^{56}Mn solution	0.01%	rectangular	$\sqrt{3}$	1	0.00%	∞
	Fit parameter for N_{sat} for counting efficiency	0.13%	normal	1	1	0.13%	∞
Combined uncertainty			normal			0.77%	∞
Expanded uncertainty			normal (k = 2)			1.55%	∞

9.2.3 Uncertainties reported by LNE-LNHB

Table 11: Component uncertainties for LNE-LNHB Mn bath measurement

Uncertainty component	Relative uncertainty	Evaluation type	Comment
γ-ray counting	0.6	A	Standard deviation of the mean of repeated measurements
γ-ray counter efficiency	0.65	B	Calibration
Neutron emission spectrum	0.55	B	Conservative estimation obtained by the difference between two Cf-252 spectra
Neutron capture probability by the manganese	0.8	B	Conservative estimation obtained by the difference between MCNP6 and Tripoli-4
Half-life $T_{1/2}$: 2.6470 (26) a	0.1	B	DDEP data
Combined standard uncertainty	1.32		Quadratic sum of all uncertainty component
Expanded uncertainty	2.64		

9.2.4 Uncertainties reported by LNMRI

Table 12: Component uncertainties for LNMRI Mn bath measurement

Component of uncertainty	Value	Uncertainty $U(x_i)$ (%)	Distribution	Divisor	Standard uncertainty $u(x_i)$ (%)
Counting	3475.832	0.21	Normal	1	0.206
Counter efficiency	5.245E-4	0.53	Normal	1	0.528
N	0.839	0.10	Rectangular	1.73	0.058
Source capture	0.085	0.25	Rectangular	1.73	0.14
Leakage	0.342	0.12	Rectangular	1.73	0.069
F	0.528	0.25	Rectangular	1	0.25
Timing		0.01	Rectangular	1.73	0.0043
Dead-time effects	5.21×10^{-7}	0.30	Normal	1	0.30
Half life of source	8.3E-9	0.00	Rectangular	1.73	3.2×10^{-5}
Combined standard uncertainty					**0.709**
Coverage factor, k					**2**
Expanded uncertainty					**1.42**

9.2.5 Uncertainties reported by NIM

Table 13: Component uncertainties for NIM Mn bath measurement

Source	Uncertainty /%	Type of uncertainties
Counting statistical	0.05	A
Background correction	0.01	A
Detection efficiency	0.72	B
Leakage	0.02	B
Oxygen and sulfur capture	0.03	B
Source and cavity capture	0.15	B
Fraction of thermal neutrons captured by ^{55}Mn	0.04	B
Combined Standard Uncertainty /%	0.74	
Expanded Uncertainty (k = 2) /%	1.5	

9.2.6 Uncertainties reported by NMIJ

As NMIJ used a relative method where the ^{252}Cf source was measured relative to an ^{241}Am-Be source their uncertainties are summarized in the following 4 uncertainty budgets

Table 14: Uncertainty budget for R_{Cf}, the neutron emission rate from the Cf-252 source at the local reference time.

quantity	unit	data	unc.	unc.rel.
c_{Cf}	s^{-1}	2.0306×10^{2}	2.1681×10^{0}	1.07 %
E_{AmBe}	-	3.6178×10^{-5}	3.0779×10^{-7}	0.85 %
$r_{Cf\ AmBe}$	-	9.9064×10^{-1}	7.9508×10^{-3}	0.80 %
R_{Cf}	s^{-1}	5.6657×10^{6}	8.9725×10^{4}	1.58 %

Table 15: Uncertainty budget for c_{Cf}, the count rate for the Cf-252 source converted at the local reference time.

quantity	unit	data	unc.	unc.rel.
v_{SPS}	-	1.0000×10^{0}	2.0000×10^{-3}	0.20 %
v_{Cf}	-	1.0000×10^{0}	1.0000×10^{-2}	1.00 %
v_{ROI}	-	1.0000×10^{0}	1.0000×10^{-3}	0.10 %
$c_{raw,Cf}$	s^{-1}	2.0306×10^{2}	6.0917×10^{-1}	0.30 %
c_{Cf}	s^{-1}	2.0306×10^{2}	2.1681×10^{0}	1.07 %

Table 16: Uncertainty budget for E_{AmBe}, the count per neutron emission from the AmBe source.

quantity	unit	data	unc.	unc.rel.
v_{Sp9}	-	1.0000×10^{0}	2.0000×10^{-3}	0.20 %
v_{AmBe}	-	1.0000×10^{0}	5.0000×10^{-3}	0.50 %
v_{ROI}	-	1.0000×10^{0}	1.0000×10^{-3}	0.10 %
c_{AmBe}	s^{-1}	3.2104×10^{2}	2.0187×10^{-1}	0.06 %
R_{AmBe}	s^{-1}	8.8740×10^{6}	5.7500×10^{4}	0.65 %
E_{AmBe}	-	3.6178×10^{-5}	3.0779×10^{-7}	0.85 %

Table 17: Uncertainty budget for $r_{Cf\ AmBe}$, the ratio of the count per neutron emission from the Cf-252 source to that from the AmBe source.

quantity	unit	Data	unc.	unc.rel.
$N_{react,Cf}$	-	3.6916×10^{-5}	1.6978×10^{-8}	0.05 %
$N_{react,AmBe}$	-	3.7265×10^{-5}	1.6773×10^{-8}	0.05 %
χ_{dens}	-	1.0000×10^{0}	3.0000×10^{-3}	0.30 %
χ_{temp}	-	1.0000×10^{0}	1.0000×10^{-3}	0.10 %
χ_{B}	-	1.0000×10^{0}	3.0000×10^{-3}	0.30 %
χ_{ver}	-	1.0000×10^{0}	3.0000×10^{-3}	0.30 %
χ_{room}	-	1.0000×10^{0}	1.0000×10^{-3}	0.10 %
$\chi_{AmBe,model}$	-	1.0000×10^{0}	5.0000×10^{-3}	0.50 %
$\chi_{AmBe,spec}$	-	1.0000×10^{0}	1.0000×10^{-3}	0.10 %
$\chi_{Cf,model}$	-	1.0000×10^{0}	3.0000×10^{-3}	0.30 %
$r_{Cf\ AmBe}$	-	9.9064×10^{-1}	7.9508×10^{-3}	0.80 %

Table 18: Component uncertainties for NIST Mn bath measurement

Term	Value	Relative uncertainty	Uncertainty type	Distribution assigned
NBS-1 rate	1.227×10^{6} s^{-1}	0.85%	B	Gaussian
Cf/NBS-1 count rate ratio	7.1320	0.042%	A	Gaussian
Correction for losses factor*	1.0090	0.24%	B	Gaussian
Combined standard uncertainty		**0.88%**		

* The uncertainty in the correction for losses factor was derived by assigning 33% uncertainty to each neutron disappearance mechanism and combining in quadrature.

Table 19: Loss term uncertainties for NIST Mn bath measurement

Neutron disappearance mechanism	NBS-1 (Ra-Be)		Am-Be	
	Value	Relative uncertainty	Value	Relative uncertainty
Fast neutron leakage	0.0000		0.0023	35%
Thermal neutron leakage	0.0000		0.0003	35%
Oxygen capture	0.0000		0.0203	30%
Sulfur capture	0.0000		0.0085	35%
Teflon capture	0.0000		0.0068	35%
Thermal source absorption	0.0027	35%	0.0014	35%
Total loss (ε)	0.0027	35%	0.0396	18%

9.2.7 Uncertainties reported by NPL

Table 20: Component uncertainties for NPL Mn bath measurement

Source	Uncertainty (%)	Distribution	Sensitivity	Uncertainty component (%)	Degrees of freedom
Counting	0.02	Normal	1	0.02	∞
Cross-section ratio	0.2	Normal	1	0.2	∞
Efficiency	0.4	Normal	1	0.4	∞
O & S losses	15	Rectangular	0.00839	0.0727	∞
Cavity and source capture	5	Rectangular	0.01936	0.0559	∞
Leakage	7	Rectangular	0.00355	0.0144	∞
Timing	0.05	Rectangular	1	0.0289	∞
Mixing	0.2	Rectangular	1	0.1155	∞
Solution concentration	0.1	Normal	1	0.1	9
Background	10	Normal	0.0009	0.0085	9
Dead-time	5	Normal	0.01416	0.1416	9
Half-life of source	0.15	Normal	0.0012	0.0001	∞
Combined standard uncertainty				**0.503**	2616

9.2.8 Uncertainties reported by NRC

Table 21: Component uncertainties for NRC Mn bath measurement. All uncertainties are assumed Gaussian.

Term	Sources of Uncertainty	Type A (%)	Type B (%)	Contribution to Emission Rate (%)
A	counting (peak-fitting, linear fit of decay)	0.3		0.3
ε	standardization	0.3		0.5
	counting (peak-fitting, linear fit of decay)		0.4	
f	bath concentration		1.9	1.4
	cross-section ratios		0.2	
	Westcott parameters		13	
(1-*L*-*O*-*S*)	oxygen, sulfur losses		1	0.2
	leakage		3	
	source capture		-	
D	half-lives, abundances		0.3	0.3
Combined Uncertainty				1.6
Expanded Uncertainty				3.2

9.2.9 Uncertainties reported by VNIIM

Table 22: Component uncertainties for VNIIM Mn bath measurement

Source of uncertainty	Value, x_i		Standard uncertainty, %	Type	Sensitivity coefficient, c_i	Contribution to the combined uncertainty, $\lvert c_i \cdot x_i \rvert$, %
Weighted average detector count rate, N_0	10039.2	s^{-1}	0.03	A	1	0.03
Correction on thermal neutrons adsorption by impurities, k_1	1.0027	rel. un.	0.03	B	1	0.03
Correction on thermal and fast neutrons adsorption by construction materials nuclei, k_2	1.0	rel. un.	0.02	B	1	0.02
Coefficient for the part of thermal neutrons captured by Mn nuclei, F	2.236	rel. un.	0.45	B	1	0.45
Mn-bath registration «efficiency», ε	0.00440	rel. un.	0.40	B	1	0.40
Correction on the neutrons leakage from the moderator, l	0.0082	rel. un.	0.2	B	$\frac{l}{1+l}$	0.007
Correction on neutrons capture in the source material, m	0.0010	rel. un.	0.8	B	$\frac{m}{1+m}$	0.0008
Correction on the fast neutrons capture by S and O nuclei, χ	0.0043	rel. un.	1.0	B	$\frac{\chi}{1+\chi}$	0.028
Combined uncertainty, u_C, %						0.6
Expanded uncertainty U, % ($k = 2$)						1.2

Table 23: Component uncertainties for VNIIM associated particles registration measurement

Source of uncertainty	Value, x_i		Standard uncertainty, %	Type	Sensitivity coefficient, c_i	Contribution to the combined uncertainty, $\|c_i \cdot x_i\|$, %
Neutron flux from the reaction ***T(d,n)^{4}He***, Φ_0	$8.82 \cdot 10^6$	s^{-1}	0.5	B	1	0.5
The area under the thermal neutrons distribution curve for the Cf-252 source, S	$4.240 \cdot 10^9$	rel. un.	0.03	A, B	1	0.03
The area under the thermal neutrons distribution curve for ***T(d,n)^{4}He***, S_0	$6.282 \cdot 10^9$	rel. un.	0.03	A, B	1	0.03
The neutron capture in the graphite from (n,α)-reaction for the Cf-252 source, K	1.002	rel. un.	0.25	B	1	0.25
The neutron capture in the graphite from (n,α)-reaction for ***T(d,n)^{4}He***, K_0	1.164	rel. un.	0.25	B	1	0.25
Combined uncertainty, u_C, %						0.6
Expanded uncertainty U, % ($k = 2$)						1.2

Table 24: Comparison of component, combined and expanded uncertainties for Mn bath measurements of all participants

Source of uncertainty	Probability distribution	CMI	KRISS	LNE-LNHB	LNMRI	NIM	NIST	NPL	NRC	VNIIM
Counting	normal	0.037	0.5	0.6	0.206	0.05	0.042	0.02	0.3	0.03
Cross section ratios	normal			0.5	0.25**	0.04**		0.2	1.4**	0.45**
Counter efficiency	normal	0.160	0.13	0.65	0.528	0.72		0.4	0.5	0.40
Oxygen and sulphur losses	rectangular	0.335*	0.5*	0.8*	0.058	0.03	0.24†	0.0727		0.028
Source and source holder capture	rectangular	*	*	*	0.14	0.15	†	0.0559		0.02
Leakage	rectangular	*	*	*	0.069	0.02	†	0.0144		0.007
Mixing	rectangular		negligible					0.1155		
Timing	rectangular	0.043	0.27		0.0043			0.0289		
Dead-time effects	rectangular	negligible	0.10		0.3			0.1416		
Half life of source	normal	0.085	negligible	0.1	3.2E-5e			0.0001		
Concentration measurement	normal/rectangular		0.15		**	**		0.1	**	**
Impurity contribution	rectangular									0.03
Manganese resonance	rectangular									
Half life of Mn-56	normal	0.031	0.018							
Mass of $MnSO_4$ solution	no assumption									
Background	normal					0.01		0.0085		
Count rate of reference source	normal						0.85			
Combined standard uncertainty	normal	0.39	0.77	1.32	0.71	0.74	0.88	0.50	1.6	0.6
Expanded uncertainty	normal ($k = 2$)	0.78	1.55	2.64	1.42	1.5	1.76	1.06	3.2	1.2

* CMI, KRISS and LNE-LNHB calculate the probability of capture by Mn, as opposed to the losses to oxygen, sulphur, source capture, leakage etc. Therefore there is only one uncertainty component rather than 3.
** LNMRI, NIM, NRC and VNIIM have a component for the uncertainty in the manganese thermal capture fraction which covers the cross section ratio and the solution concentration.
† The value of 0.24% corresponds to the correction for losses factor that NIST apply to correct for the differences in losses between the Cf source and their reference Ra-Be source

Note that the component uncertainties given in the table include sensitivity coefficients and so may not be directly comparable, e.g. the uncertainty component for source and source holder capture is dependent on the construction of the source holder used by each participant.

9.3 Appendix C: Descriptions of the neutron emission rate measurement techniques of the laboratories

9.3.1 CMI

The CMI manganese bath is a sphere 100 cm in diameter and contained $MnSO_4$ solution with a concentration of 20.93%, corresponding to a density of 1.2317 $g.cm^{-3}$ and a hydrogen to manganese number density ratio (N_H/N_{Mn}) of 63.33 for the intercomparison measurements.

The source was placed at the centre of the bath for approximately 10 half-lives of ^{56}Mn. The source was then removed and replaced at the centre by a NaI(Tl) scintillation detector ∅16 mm × 16 mm to count the decay of the solution. The solution was stirred thoroughly for about 20 minutes before counting began. Two measurements of the intercomparison source were performed.

The efficiency of the CMI manganese bath system was determined by adding reactor activated ^{56}Mn solution to the bath. The specific activity of the ^{56}Mn solution was determined by 4πβ-γ coincidence counting.

The Monte Carlo radiation transport code MCNP version 6.1.1 with ENDF/B-VII.1 cross-sections was used to calculate the probability of neutron absorption by Mn nuclei in the bath per neutron emitted from the source. This took account of neutron escape, neutrons captured by the source materials and its mounting assembly and neutrons that undergo reactions with hydrogen, oxygen and sulphur in the solution of the bath, rather than determining these fractions separately. The influence of impurities claimed by the Manganese Sulfate Monohydrate supplier on the calculation results was found insignificant.

The long-term stability of the system is checked using a reference Am-Be source.

9.3.2 KRISS

The KRISS manganese bath is a sphere 125 cm in diameter. A solution with a gravimetrically determined number density ratio (N_H/N_{Mn}) of 179.11 was used for the measurements.

During the measurement, the solution was circulated through a shielded Marinelli beaker-type detector bath equipped with a NaI(Tl) detector placed at the central hole of the beaker. The source remained in the bath for about 24 hours, after which the decay of the solution was used to determine the detector count rate at saturation. Four measurements of the intercomparison source were performed with the final result coming from a mean of all four values.

The efficiency of the manganese bath system was determined using the KRISS reference ^{241}Am-Be source (AMN24) as the research reactor used previously was unavailable. The reference ^{241}Am-Be source had previously been measured (in 2005 and 2009) when the Mn bath was calibrated using reactor-activated ^{56}Mn dissolved into a solution and added to the bath with the specific activity of the ^{56}Mn solution determined by 4πβ-γ coincidence counting.

MCNPX version 2.7.0 was used to calculate the probability of ^{56}Mn production per neutron emitted from the source. This took account of neutron leakage, neutron capture by the source materials and its mounting assembly, the neutron reactions with hydrogen, oxygen and sulphur nuclei, and epithermal capture by the manganese nuclei. ENDF/B-VII cross-sections were used. Impurities in the solution were not considered and believed to be negligible.

The long-term stability of the system was checked using the reference Am-Be source.

9.3.3 LNMRI

The LNMRI manganese bath is a static system where after the source has irradiated the solution to saturation a NaI(Tl) scintillator is placed at the centre of the bath to measure the decay. The bath is a sphere 100 cm in diameter. Each decay measurement was considered with data from 30 consecutive counts of 500 seconds each. Acquisition data was obtained with a MCA connected to the detector and a computer. The manganese number density ratio N_H/N_{Mn} = 35.26 was determined through a gravimetric method. Impurities in the solution were measured by ICP-MS method and were considered negligible. MCNPX version 2.7.0 was used to calculate fast neutron capture, neutron leakage from bath solution and neutron capture by source material encapsulations.

9.3.4 LNE-LNHB

The LNE-LNHB manganese bath is a thin-walled stainless steel sphere of 100 cm in diameter, filled with a solution of manganese sulphate with a density of 1.277 g cm^{-3} (measured with a calibrated densitometer). The hydrogen to manganese number density ratio (N_H/N_{Mn}) in the solution time was 52.2 at the measurement time.

The neutron source was placed in the centre of the bath in a cylindrical PMMA holder. The solution was stirred and circulated continuously between the bath and an external detector assembly containing a NaI(Tl) scintillation detector which is used to measure the induced activity of ^{56}Mn at saturation. The detection system was previously calibrated using a concentrated ^{56}Mn solution standardized by the TDCR (triple to double coincidence ratio) method.

Corrections for the leakage fraction, the capture in the source and source mounting assembly, and the capture by (n,p) and (n,α) reactions in sulphur and oxygen, and thermal neutron capture by nuclei other than manganese were calculated using MCNP6 with ENDF/B-VII cross-sections. Impurities in the solution were not considered.

9.3.5 NIM

The NIM manganese bath is a sphere 110 cm in diameter and contained a solution with a hydrogen to manganese number density ratio (N_H/N_{Mn}) of 59.704 for the comparison measurements. N_H/N_{Mn} was determined gravimetrically (i.e. comparing the mass of a sample of the solution with the mass of the residue after evaporation) and by measuring the density of the solution.

The neutron source was placed in the centre of the bath in a tube with an inner diameter of 14 mm made of 1 mm thick stainless steel. The solution was circulated continuously between the bath and a shielded sample vessel with two ∅40 mm × 40 mm NaI(Tl) scintillation detectors mounted one at either side. After 48 hours, ten measurements of 600 seconds duration were made of the solution activity with each NaI detector.

The efficiency of the NIM manganese bath system was determined using ^{56}Mn produced by activation in a reactor. It was then dissolved into a solution and added to the bath. The specific activity of the ^{56}Mn solution was determined by 4$\pi\beta$-γ coincidence counting.

Corrections were made for neutron leakage, fast neutron losses due to interactions in the oxygen and sulphur, and thermal neutrons absorbed by the neutron source and the container using MCNP 4C with ENDF/B-VII cross-sections. Thermal neutron capture by manganese was also calculated using MCNP.

9.3.6 NIST

The NIST manganese bath is operated in comparison mode where the neutron emission rate of an unknown source is compared with that of a 37 GBq Ra-Be photoneutron source (NBS-1), the US national neutron reference which has been calibrated multiple times using a variety of means and shows excellent stability[10],[11],[12]. The bath is a sphere 129 cm in diameter and the solution had a specific gravity (relative density to water) of 1.253 for the intercomparison measurements.

One measurement was made of the intercomparison source with measurements of NBS-1 made 2 weeks before and two weeks after. Each source was left in the manganese bath for several days while diverting a small flow of the solution into a Marinelli beaker with a NaI scintillator positioned inside to count the ^{56}Mn activity.

Corrections were applied to allow for the difference in the leakage fraction, the capture in the source and source mounting assembly, and the fast neutron capture by sulphur and oxygen. The corrections were calculated using MCNP6.2 with ENDF/B-VII cross-sections for all reactions except ^{16}O(n,α) where ENDF/B-VI was used.

9.3.7 NMIJ

The NMIJ calibration method is based on relative measurements with respect to a 148 GBq AmBe neutron source calibrated at NPL. The reference source and the source to be calibrated are placed in turn at a predetermined position near the centre of a graphite pile (230 cm wide, 190 cm deep and 190 cm high) consisting of reactor-grade graphite blocks stacked on a base iron board on a concrete floor. A spherical ^{3}He proportional counter is placed in a channel running 90 cm from the source position. Neutrons emitted from a neutron source located near the centre of the graphite pile get thermalized as they move away from the source, and the thermalization is almost complete at a distance of 90 cm. A thermal neutron detector is placed in a region where the neutrons are sufficiently thermalized and will produce a count rate that is almost solely proportional to the neutron emission rate, with little dependence on the energy distribution of the neutrons emitted from the source. Therefore, the neutron emission rate of the calibration item can be determined from the ratio of the count rate between the reference source and the calibration item placed at a predetermined position near the centre of the graphite pile.

9.3.8 NPL

The NPL manganese bath is a sphere 98 cm in diameter. Solution with hydrogen to manganese number density ratios (N_H/N_{Mn}) of 34.37 and 34.46 was used for the 2016 and 2021 measurements respectively. The concentration was determined gravimetrically in each case.

The solution was continuously circulated through a shielded reservoir where two NaI scintillators were used to measure the activity of the solution, before being pumped back into the bath. The saturated count rate was obtained from the counting cycles when the source was in the bath as well as from those after the source had been removed. Both NPL measurements consisted of two separate bath irradiations performed within a week of each other.

The NaI detectors were calibrated by adding an active solution of ^{56}Mn to the bath, the activity concentration of which had been determined using an ion chamber. A linear fit is made to the efficiency measurements to interpolate or extrapolate to the day of a neutron source measurement.

MCNP5 was used to calculate the leakage fraction, the capture in the source and source mounting assembly, and the capture by (n,p) and (n,α) reactions in sulphur and oxygen using ENDF/B-VI cross-sections where available. Thermal neutron capture by hydrogen, sulphur, and solution impurities was calculated using thermal cross sections with appropriate Westcott parameters to allow for epithermal resonance capture. A hydrogen to manganese cross-section ratio derived from measurements at different dilutions in the NPL manganese bath[13] was used. The impurity levels were taken from a chemical analysis of the solution.

9.3.9 NRC

The NRC manganese bath is a spherical cavity composed of fiberglass and has a diameter of 1 m. The solution is static and has a manganese component of (9.64 ± 0.19) % as determined by the Chemical Metrology Group at the NRC, using inductively coupled plasma induced mass spectroscopy (ICP-MS) method. The value of the ratio of hydrogen to manganese is therefore $N_H/N_{Mn} = 46.6 \pm 0.9$. The neutron source is inserted into the bath via a source holder composed of ABS plastic. The cylindrical holder has a radius of 1.25 cm and a height of 5 cm. A sodium iodide (NaI) detector with a radius of 6.35 cm and height of 5.08 cm is used to measure the induced ^{56}Mn. The detector rests at the top of the bath after extraction of the neutron source. The data is acquired from the NaI using a Canberra Multichannel Analyzer and the gamma spectrum recorded using the Canberra Genie 2000 Software. The neutron source was placed in the bath 3 times, each irradiation lasting approximately 24 hours.

The NRC manganese bath is calibrated by inserting a standardized source of $^{56}MnSO_4$ to the bath and counting the decay. To produce ^{56}Mn, a sample of potassium permanganate ($KMnO_4$) is exposed to a thermal neutron flux at the Royal Canadian Military (RMC) SLOWPOKE-2 Facility, forming insoluble manganese dioxide ($^{56}MnO_2$). The manganese dioxide is extracted using a Büchner funnel and glass filter, and rinsed using a solution of hydrogen peroxide and sulfuric acid to produce the required $^{56}MnSO_4$ solution. Sources of the active sample of $MnSO_4$ are simultaneously prepared for measurement with a primary standard for radio-nuclides ($4\pi\beta$-γ counter) and for insertion into the bath. A second primary standard, a liquid scintillation counter, was used as a consistency check.

The components of the (1-L-O-S) term were determined using MCNP6 with the ENDF-VII.1 libraries. Thermal neutron capture by hydrogen, sulphur, and solution impurities was calculated using thermal cross sections with appropriate Westcott parameters to allow for epithermal resonance capture

9.3.10 VNIIM

9.3.10.1 Mn bath method

The VNIIM bath is a cylinder 85 cm in diameter. Two irradiations of the solution were performed; one of 26.312 hours and another of 63.136 hours. The activity of the solution was derived from the gamma count rate of a NaI(Tl) scintillation detector placed at the centre of the bath after the source had been removed. The efficiency of the system was determined using active manganese solution.

9.3.10.2 Associated particles method

The neutron source emission rate was determined using the all-wave graphite comparator[14] relative to the neutron fluence rate from T(d,n)^{4}He determined by associated alpha particle counting. The comparator consists of a graphite sphere, 4 m in diameter, with a central spherical cavity, 0.4 m in diameter, in which the source was located.

Measurements were made using a ^{3}He thermal neutron detector at 38 different distances from the centre of the sphere. The epithermal neutron contribution for each position was corrected for by making measurements with the detector under cadmium.

Corrections were made for (n,α) capture in the graphite from the ^{252}Cf source and the T(d,n)^{4}He reaction using a Monte Carlo method. Allowance was also made for neutron capture in the target chamber shell.

9.4 Appendix D: Anisotropy measurements

CMI, KRISS, LNE-LNHB, NIM, NPL and VNIIM measured the anisotropy of the source in addition to the emission rate. KRISS, LNE-LNHB, NIM, NPL and VNIIM made measurements at 10° steps from 0° to 180°, whereas CMI made measurements at 2° steps over the same range. The convention used to define the angles around the source capsule is shown in figure 4.

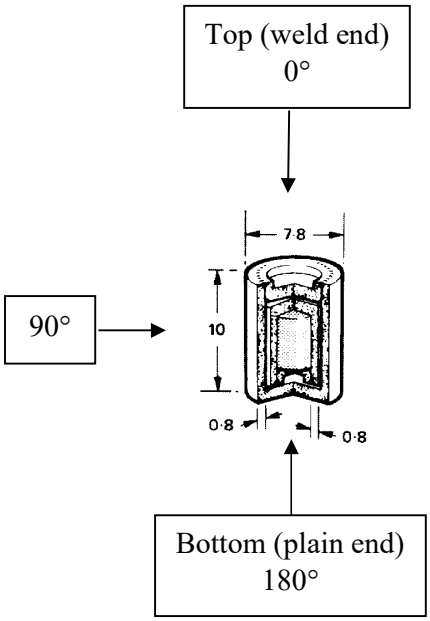

Figure 4: Anisotropy angle convention for the intercomparison source

9.4.1 CMI

The anisotropy factor was determined by using an SP9 ^{3}He proportional counter placed in a polyethylene moderating sphere 7" (17.78 cm) in diameter. The distance between the axis of the source rotation and the centre of the sphere was equal to 100 cm. The stand for the source rotation was laser levelled to ensure that the source axis remained in the horizontal plain during rotation. Detector count rates at each angle θ_i were calculated from a mean of 10 values corresponding to 5 full rotations and two angles (θ_i and 360° - θ_i). To derive the anisotropy factor at 90° the average count rate of the 5 mean values from 86° to 94° was used. The count rate at each angle was corrected for scatter using the same value, determined by the generalized fit method as a mean value for a ^{252}Cf source oriented at 90° and 0°.

9.4.2 KRISS

The anisotropy of the neutron source was measured using an SP9 ^{3}He proportional counter inside an 8" Bonner sphere. The distance from the source to the 8" Bonner sphere was 1.5 m. The Cf source was rotated from 0° to 360° in 10° steps. Count rates from 0° to 180° were obtained by summing those from the same polar angles, assuming cylindrical symmetry. A scatter correction was made using the shadow cone technique.

9.4.3 LNE-LNHB

The anisotropy of the neutron source was measured using a BF_3 long counter at a distance from the source of about 1.5 m. The source was placed on a lightweight holder positioned on top of a rotating support with its cylindrical axis in the horizontal plane. A scatter correction was made by making measurements with a shadow cone positioned between the source and the long counter.

9.4.4 NIM

The anisotropy measurement was made using a long counter. The central detector of the long counter is a BF_3 proportional counter (Type 34EB70/38, made by Centronic). The source is placed and fixed on a swinging strut, the central axis of the source and the long counter is at height 1.8m above the floor, the distance between the source center and the front surface of long counter is 1.5m. The scattered neutrons are not corrected because the variation of the scatter fraction is very small at different angles. 10 measurements of 100 seconds were made for each angle.

9.4.5 NPL

The source was placed on a light-weight holder at the centre of a low scatter area with its cylindrical axis in the horizontal plane. The holder was fixed to a rotating stage enabling the source to be rotated through 360°. Measurements were made with a long counter of the McTaggart type[15], built at NPL, with a 50 mm outer diameter BF_3 tube, at a distance of 199.9 cm from the source. Relative neutron emission rates were measured over the angular range 0° to 360° relative to the cylindrical axis of the source, in steps of 10°, both with and without a shadow cone to enable the scatter contributions to be subtracted. The measurements from 0° to 180° were combined with those at the corresponding angles from 180° to 360° i.e. 360° and 0°, 350° and 10°, 340° and 20° etc.

9.4.6 VNIIM

A long counter at 1.2 m from the source was used to measure the anisotropy of the source which was placed on a thin rotating rod. The source was rotated from 0° to 180° in 10° steps. The scatter contribution was measured using a boron loaded polyethylene shadow cone between the source and the detector.

9.4.7 Results

The measurements of all six laboratories are shown in Figure 5. All are normalised to the sum of the angular measurements weighted according to the solid angle over the angular interval.

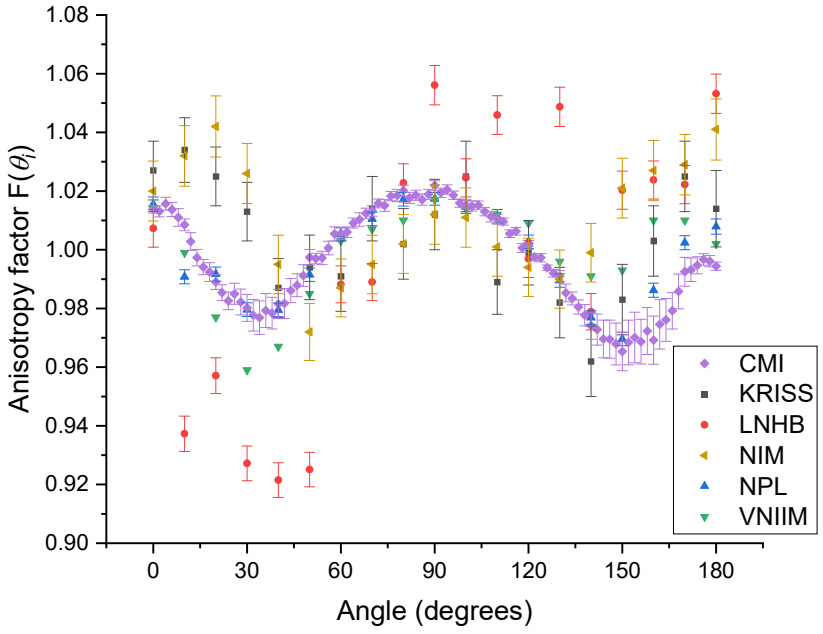

Figure 5: Graph of anisotropy factor vs angle

(error bars represent the combined uncertainty at $k = 1$)

It can be seen that there is good agreement between CMI and NPL over the majority of the range of angles, and between CMI, KRISS, NIM, NPL and VNIIM over a more limited range of angles. The majority of the LNE-LNHB measurements appear to be outliers and no numerical errors were found when they were asked to check their results.

The angle of most significance is 90° as this is the conventional angle for positioning any instrument or device being irradiated by the source. The anisotropy factors of each laboratory at 90°, $F(90°)$, are given in Table 25 and plotted in Figure 6. The agreement is good with the exception of the LNE-LNHB value. As no uncertainties were reported by VNIIM it was not possible to derive a weighted mean which may well differ from the simple mean due to the large difference in uncertainties between the values.

Table 25: Anisotropy factors at 90° with combined uncertainties at $k = 1$

	$F(90°)$
CMI	1.0196 ± 0.0019
KRISS	1.012 ± 0.012
LNE-LNHB	1.0561 ± 0.0067
NIM	1.012 ± 0.010
NPL	1.0174 ± 0.0022
VNIIM	1.017

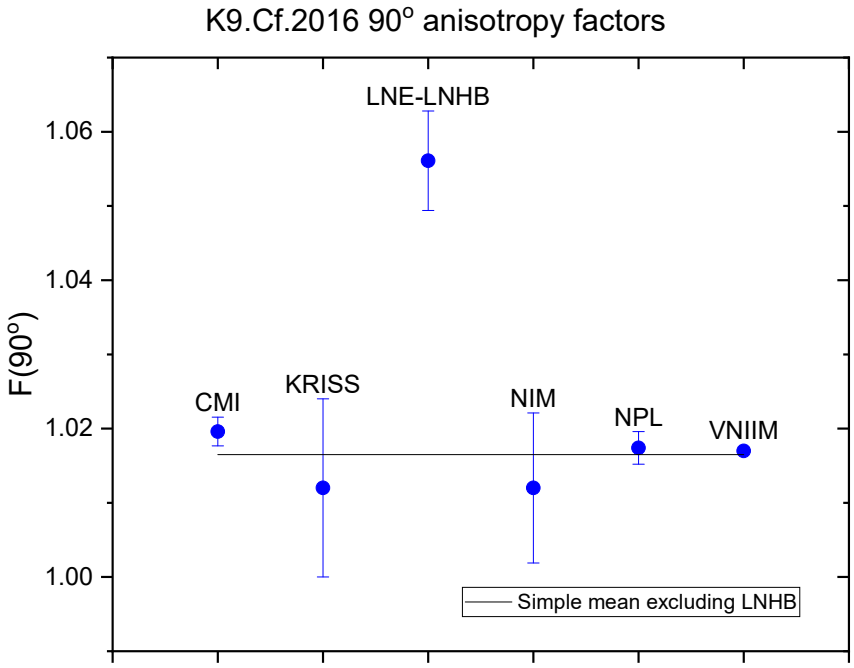

Figure 6: Plot of anisotropy factors at 90° with combined uncertainties at $k = 1$

A possible explanation for the differences seen between some of the participants over parts of the angular range could be that the source material is not located centrally within the inner capsule. It may be off-axis, diagonally orientated or free to move within the inner void. If that is the case then the anisotropy measurements would be different if the source was not placed in the same rotational orientation by each participant. As there were no orientating marks on the capsule and the rotational orientation was not mentioned in the protocol it is likely that each participant mounted the source in a slightly different rotational position. The NPL measurements were an average of those from 0° to 180° and 360° to 180°, but the separate measurements show large differences for angles other than 0°, 60° to 120°, and 180° as shown in Figure 7. CMI and KRISS also made measurements over the entire angular range from 0° to 360° and averaged the readings at corresponding angles.

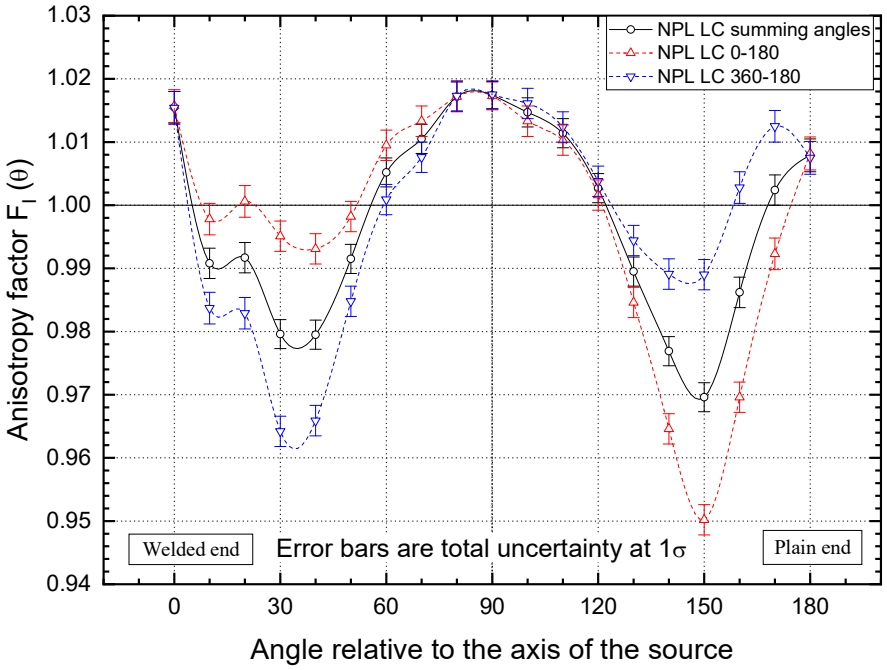

Figure 7: Graph of anisotropy factors vs angle from the NPL measurements from 0° to 180°, 360° to 180°, and the summation of the two

10 REFERENCES

1 Naggiar, V. Rapport sur la comparaison internationale de la mesure du taux d'émission de la source de neutrons Ra-Be (α,n) du Conseil National de Recherches n° 200-1 par la méthode de ralentissement des neutrons dans une solution de sulfate de manganèse, *in Recueil de Travaux du BIPM*, Vol. 1, 1966-1967

2 Axton E J, Intercomparison of Neutron-Source Emission Rates (1979-1984), *Metrologia*, **23**, 129-144, 1987. Available at https://doi.org/10.1088/0026-1394/23/3/002

3 Private communication from QSA Global Inc

4 Roberts N J and Jones L N. The content of ^{250}Cf and ^{248}Cm in ^{252}Cf neutron sources and the effect on the neutron emission rate, *Radiat. Prot. Dosim.* **126**, No. 1-4, 83-88, 2007, doi:10.1093/rpd/ncm017

5 IAEA Technical Report Series No 261, Decay data of the transactinium nuclides, IAEA, Vienna (1986)

6 IAEA Nuclear Data Services, https://www-nds.iaea.org/

7 Santi P and Miller M, Re-evaluation of Prompt Neutron Emission Multiplicity Distributions for Spontaneous Fission, *Nucl. Sci. Eng*. 160 (2008) 190–199. Available at https://doi.org/10.13182/NSE07-85

8 Axton E J and Bardell A G, Neutron Yield from the Spontaneous Fission of ^{252}Cf, *Metrologia* **21**, 59-74, (1985). Available at https://doi.org/10.1088/0026-1394/21/2/003

9 Cox M G, The evaluation of key comparison data *Metrologia* **39** 589–95, 2002. Available at https://doi.org/10.1088/0026-1394/39/6/10

10 De Juren J A, Padgett D W, and Curtiss L F. Absolute calibration of the national bureau of standards photoneutron standard: I. *J. Res. NBS*, 55(2):63–69, 1955. Available at https://nvlpubs.nist.gov/nistpubs/jres/55/jresv55n2p63_A1b.pdf

11 De Juren J and Chin J. Absolute calibration of the national bureau of standards photoneutron standard: II. Absorption in manganese sulfate. *J. Res. NBS*, 55(6):311–316, 1955. Available at https://nvlpubs.nist.gov/nistpubs/jres/55/jresv55n6p311_A1b.pdf

12 Noyce R H, Mosburg, Jr. E R, Garfinkel S B, and Caswell R S. Absolute calibration of the national bureau of standards photoneutron standard: III. Absorption in a heavy water solution of manganous sulphate. *Reactor Sci. Technol. (J. Nucl. Energy Parts A/B)*, 17:313–319, 1963. Available at https://doi.org/10.1016/0368-3230(63)90080-6

13 Axton E J, Bardell A G, Felgate S J, Long S M R, The Ratio of the Thermal Neutron Capture Cross-Sections for Hydrogen and Manganese and its Impact on the Measurement of Neutron Source Emission Rates by Manganese Bath Techniques, *Metrologia* **21** pp181-91, 1985. Available at https://doi.org/10.1088/0026-1394/21/4/003

14 VNIIM, A brief description of the VNIIM's facilities for measuring of neutron flux and neutron fluence rate, CCRI(III)/01-14, presented at CCRI(III) 14th meeting in May 2001, http://www.bipm.fr/cc/CCRI(III)/Allowed/14/CCRI(III)01-14.pdf

15 McTaggart M H, *A Study of the Neutron Long Counter*, AWRE report NR/A-1/59, 1959.